Supporting information for:

Synthesis and Excited State Modulation of Organic Blue light Emitters Based on 2,4,6-Triphenyl-1,3,5-triazine and Carbazole Derivatives through ortho-Positioned Linking Models

Xiong Li [1], Lifeng Zheng [2], Wei Tang [1], Shanghui Ye [1], Jing Ma [2], Hongji Jiang [1]

[1] State Key Laboratory of Organic Electronics and Information Displays and Jiangsu Key Laboratory for Biosensors, Jiangsu National Synergetic Innovation Center for Advanced Materials, Institute of Advanced Materials, Nanjing University of Posts and Telecommunications, Nanjing

[2] Key Laboratory of Mesoscopic Chemistry of MOE, Jiangsu Key Laboratory of Advanced Organic Materials, School of Chemistry and Chemical Engineering, Nanjing University, Nanjing

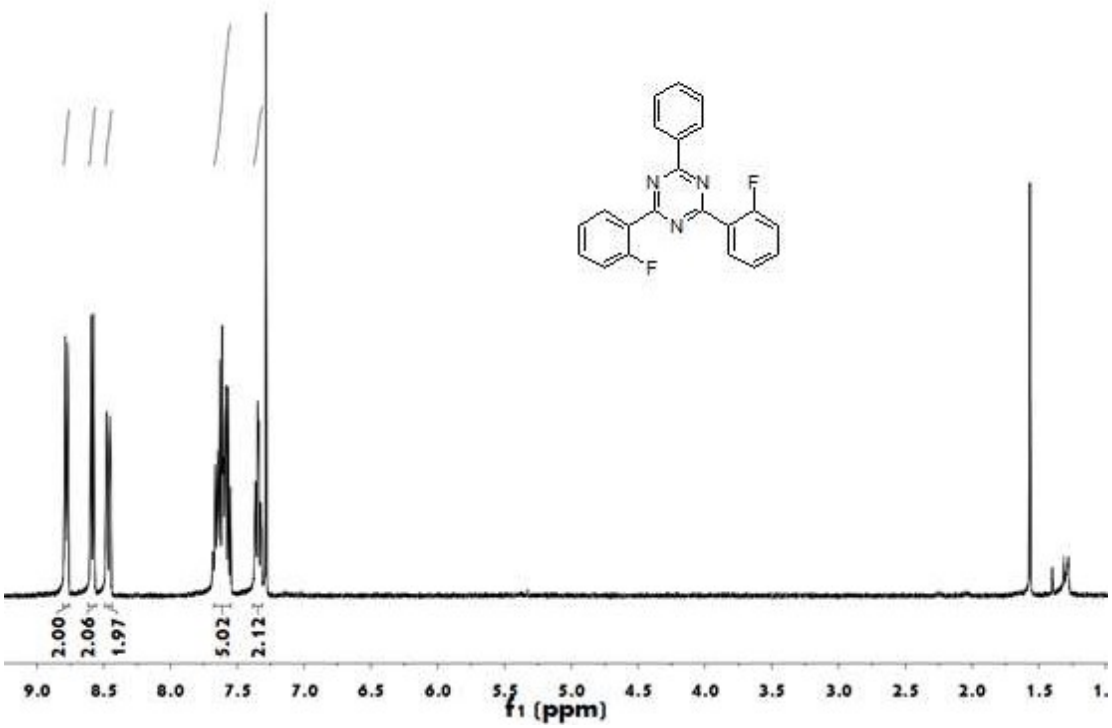

Figure S1. The ^{1}H-NMR ($CDCl_3$, 400 MHz, ppm) shift spectra of compound 2,4-bis (4-fluorophenyl) -6-phenyl-1,3,5-triazine

Corresponding author. E-mail: iamhjjiang@njupt.edu.cn

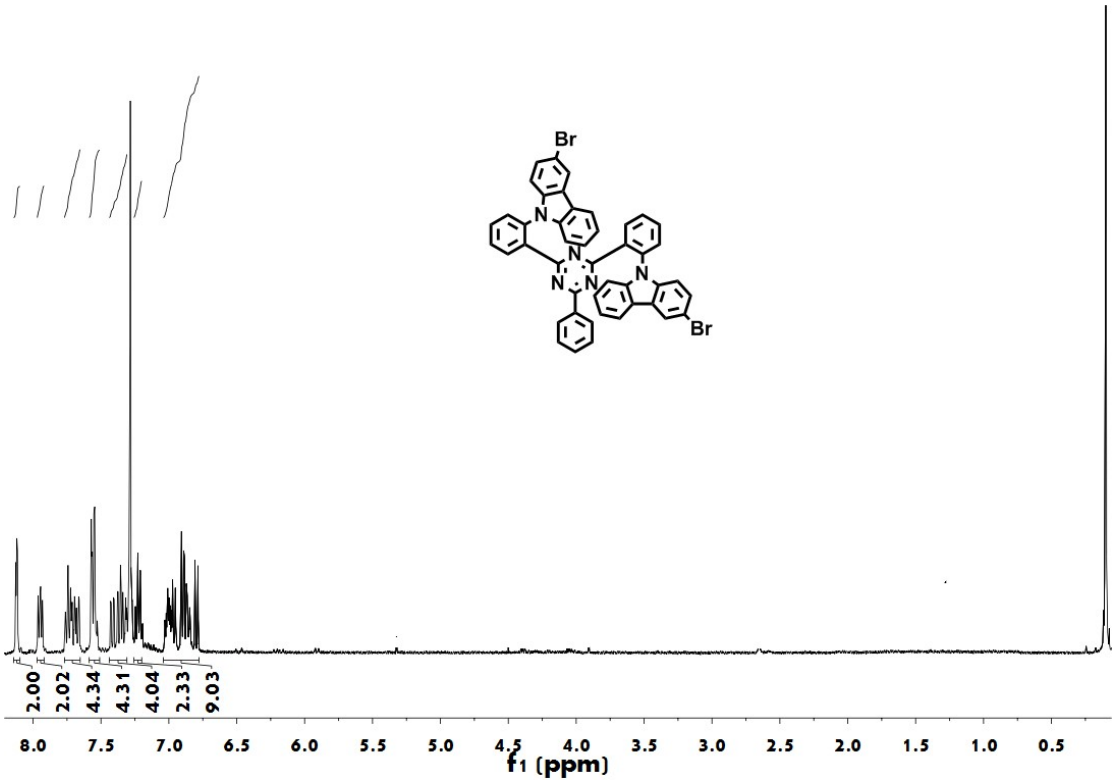

Figure S2. The ^{1}H-NMR ($CDCl_3$, 400 MHz, ppm) shift spectra of emitter 9,9 '-((6-phenyl-1,3,5-triazine-2,4-diyl) bis (2,1-phenylene)) bis (3-bromo-9H-carbazole)

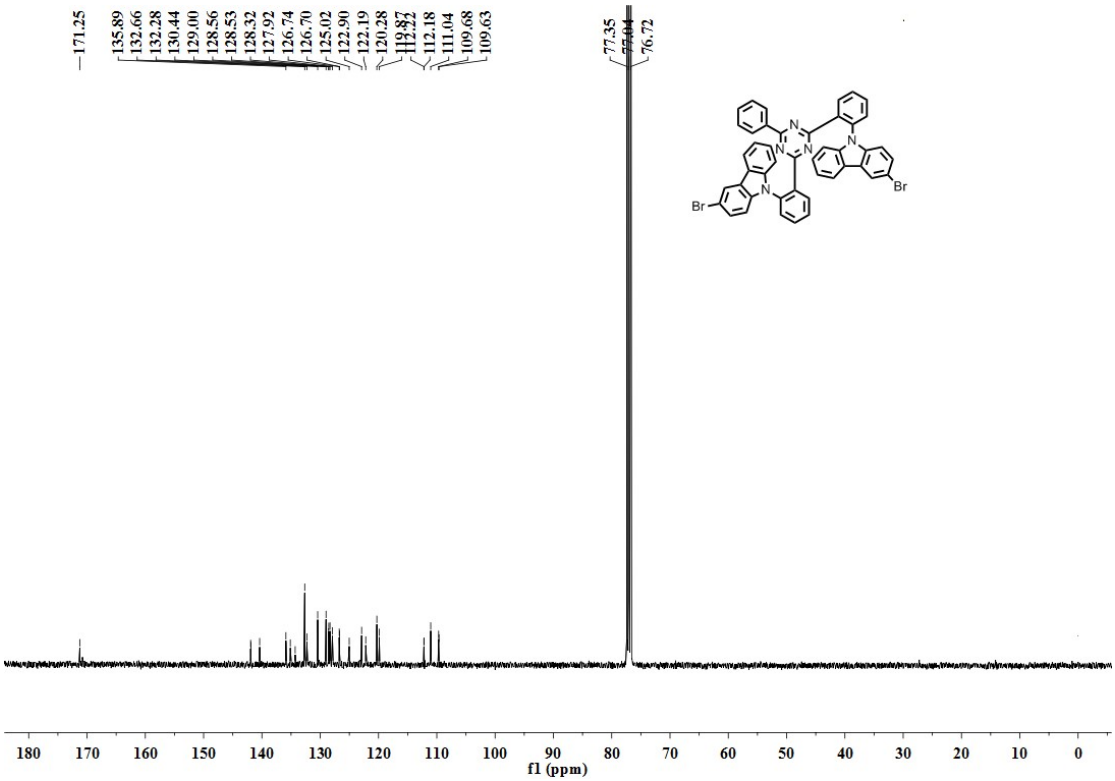

Figure S3. The ^{13}C-NMR ($CDCl_3$, 100 MHz, ppm) shift spectra of emitter 9,9 '-((6-phenyl-1,3,5-triazine-2,4-diyl) bis (2,1-phenylene)) bis (3-bromo-9H-carbazole)

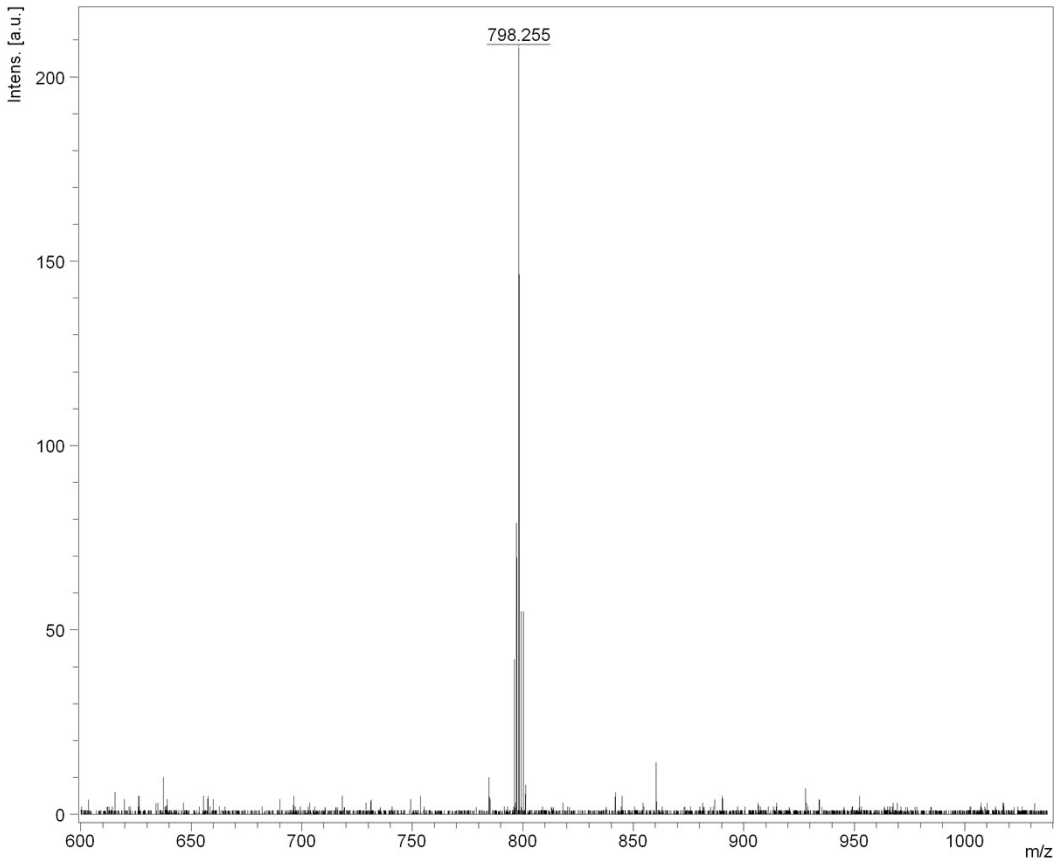

Figure S4. The MALDI-TOF spectra of emitter 9,9 '-((6-phenyl-1,3,5-triazine-2,4-diyl) bis (2,1-phenylene)) bis (3-bromo-9H-carbazole**)**

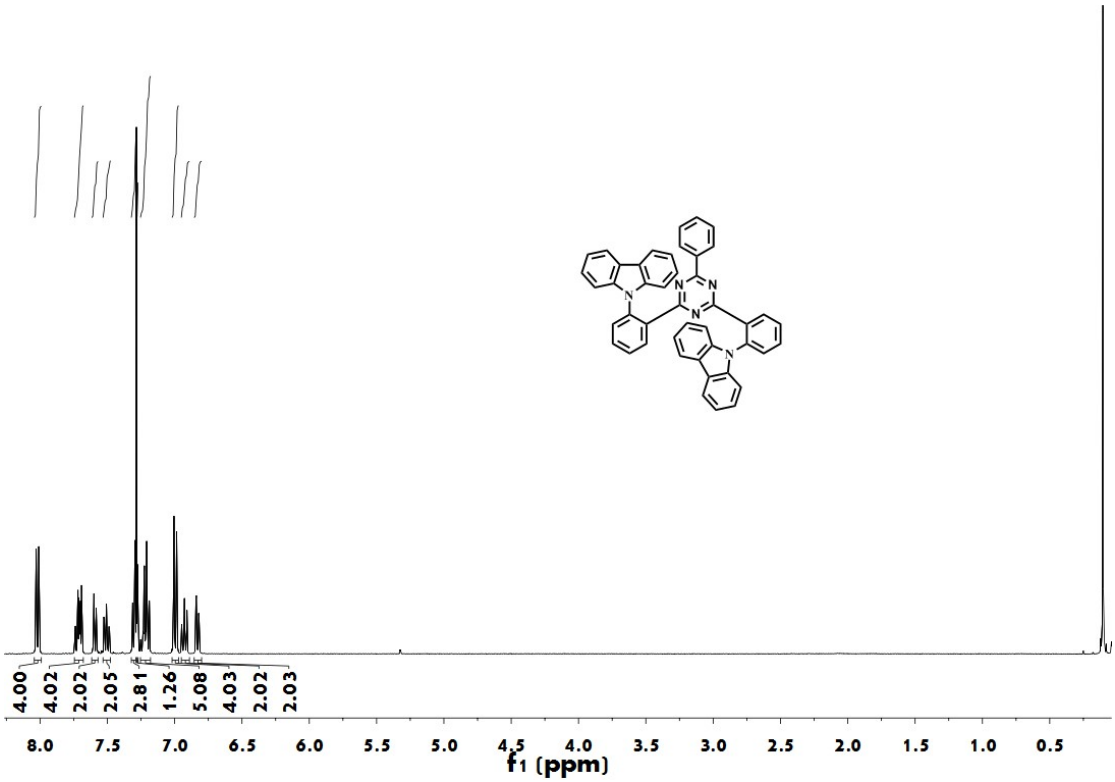

Figure S5. The ^{1}H-NMR ($CDCl_3$, 400 MHz, ppm) shift spectra of emitter 9,9 '-((6-phenyl-1,3,5-

triazine-2,4-diyl) bis (2,1-phenylene)) bis (9H-carbazole)

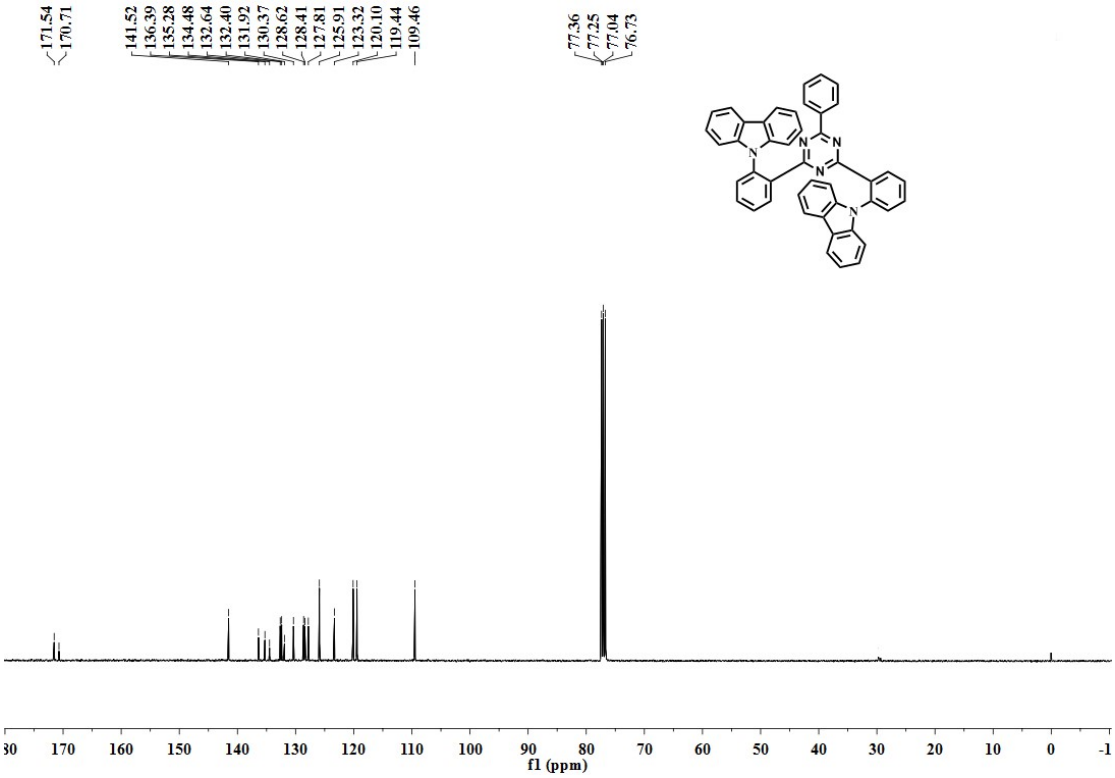

Figure S6. The ^{13}C-NMR ($CDCl_3$, 100 MHz, ppm) shift spectra of emitter 9,9 '-((6-phenyl-1,3,5-triazine-2,4-diyl) bis (2,1-phenylene)) bis (9H-carbazole)

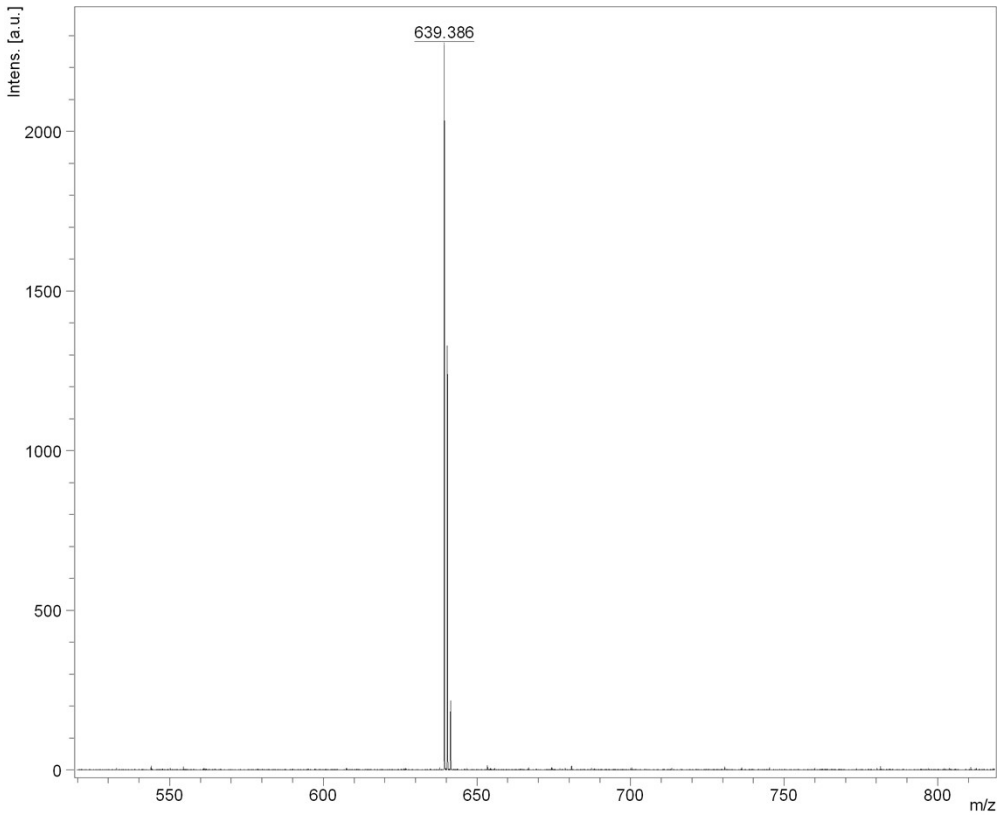

Figure S7. The MALDI-TOF spectra of emitter 9,9 '-((6-phenyl-1,3,5-triazine-2,4-diyl) bis (2,1-

phenylene)) bis (9H-carbazole)

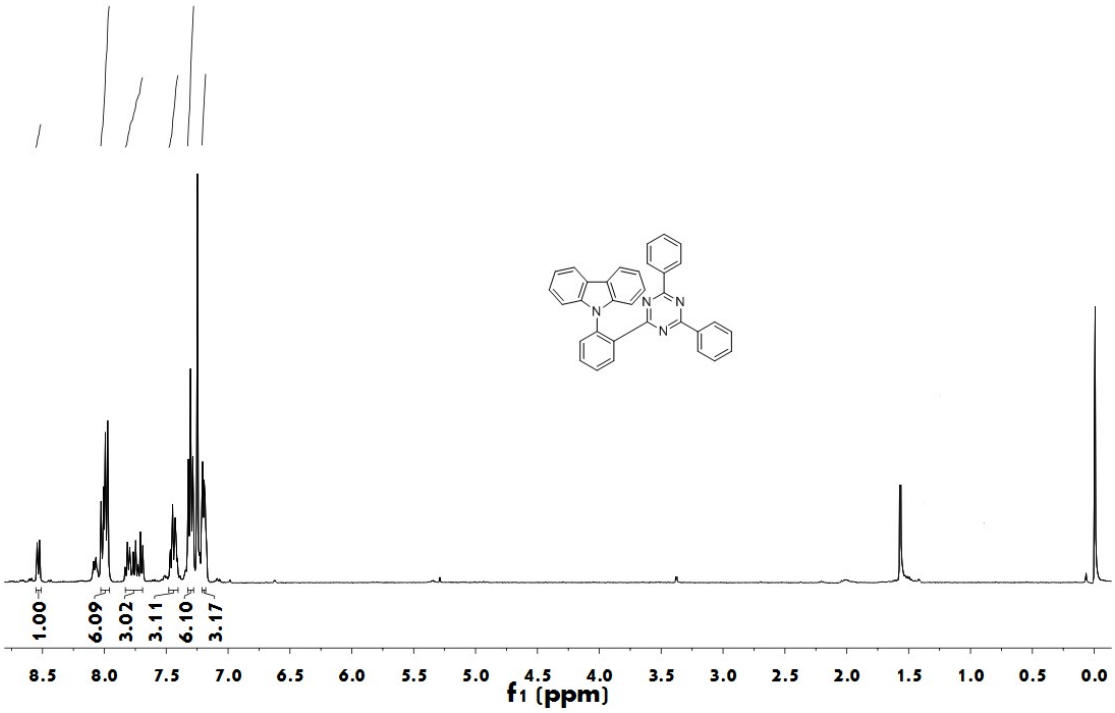

Figure S8. The ^{1}H-NMR ($CDCl_3$, 400 MHz, ppm) shift spectra of emitter 9- (2- (4,6-diphenyl-1,3,5-triazin-2-yl) phenyl) -9H-carbazole

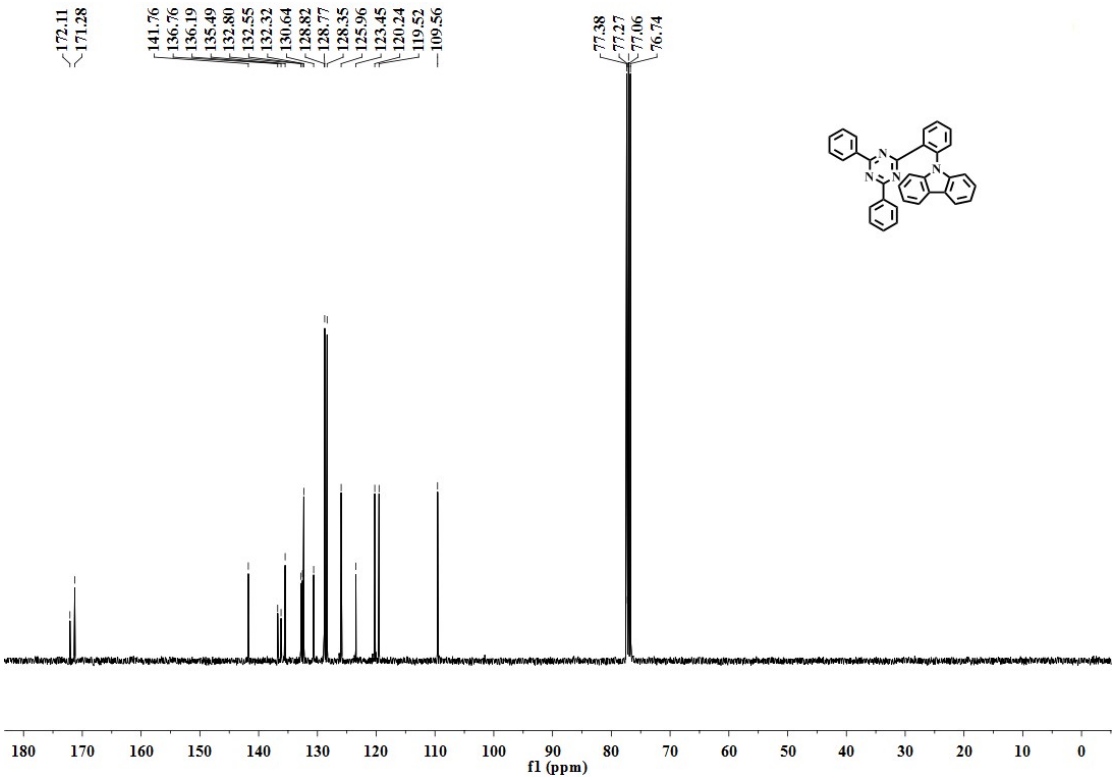

Figure S9. The ^{13}C-NMR ($CDCl_3$, 100 MHz, ppm) shift spectra of emitter 9- (2- (4,6-diphenyl-

1,3,5-triazin-2-yl) phenyl) -9H-carbazole

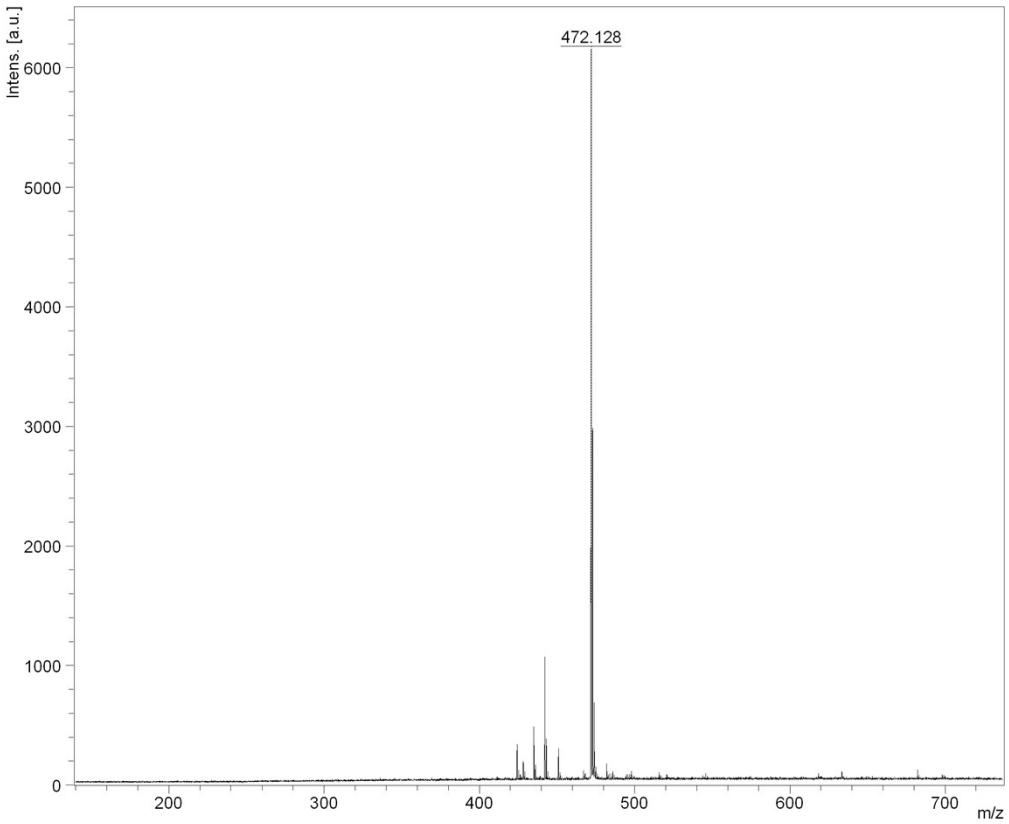

Figure S10. The MALDI-TOF spectra of emitter 9- (2- (4,6-diphenyl-1,3,5-triazin-2-yl) phenyl) -9H-carbazole

Synthesis

2-- (2-fluorophenyl)-4,6-diphenyl-1,3,5-triazine (OSTrPhF) [24]**:** 2-chloro-4,6-diphenyl-1,3,5-triazine (2.67 g, 10 mmol), 2-fluorophenylboronic acid (2.1 g, 15 mmol), $Pd(PPh_3)_4$ (420 mg, 0.6 mmol), tetrabutylammonium bromide (1.6g, 5 mmol), potassium carbonate aqueous solution (20 ml, 2 mol/L, deoxygenation) and toluene (60 ml, deoxygenation) were added to the double-necked flask. It was drained three times, protected from light at 90 °C for 24 hours in an atmosphere of N_2. After the reaction solution was cooled to room temperature, the resulting mixture was extracted with dichloromethane and water for 3 times, filtered, and concentrated under reduced pressure. The residue solid was purified by silica gel column chromatograph (petroleum ether: dichloromethane=10:1 in volume) to obtain 2.78g white solid in a yield of 85%.^{1}H NMR (400 MHz, $CDCl_3$) δ 8.79-8.71 (m, 4H), 8.47 (td, 1H), 7.62-7.52 (m, 7H), 7.34 (ddd, 1H), 7.25 (dt, 1H).

9- (2- (4,6-diphenyl-1,3,5-triazin-2-yl) phenyl) -9H-carbazole (OSTrPhCz) [22]**:** carbazole (1.5 g, 6 mmol), Cs_2CO_3 (2.1 g, 4 mmol) and compound **OSTrPhF** (1.35 g, 4 mmol) were dissolved in 50 mL N,N-dimethylformamide, poured into reaction flask, and stirred at 160 °C for 12 hours. After the reaction solution was cooled to room temperature, the resulting mixture was extracted with dichloromethane and water for 3 times, filtered, and concentrated under reduced pressure. The residue solid was purified by silica gel column chromatograph (petroleum ether: dichloromethane = 5:1 in volume) to obtain 1.13g white solid in a yield of 59.7%.^{1}H NMR (400 MHz, $CDCl_3$) δ 8.53 (d, 1H), 8.00 (dd, 7.9 Hz, 6H), 7.83 – 7.69 (m, 3H), 7.47 – 7.39 (m, 3H), 7.30 (t, 6H), 7.21 – 7.17 (m, 3H). ^{13}C NMR (400 MHz, $CDCl_3$) δ 172.11, 171.28, 141.76, 136.76, 136.19, 135.49, 132.80, 132.55, 132.32, 130.64, 128.82, 128.77, 128.35, 125.96, 123.45, 120.24, 119.52, 109.56. m/z: theoretical: 474.567, experimental: 472.168.

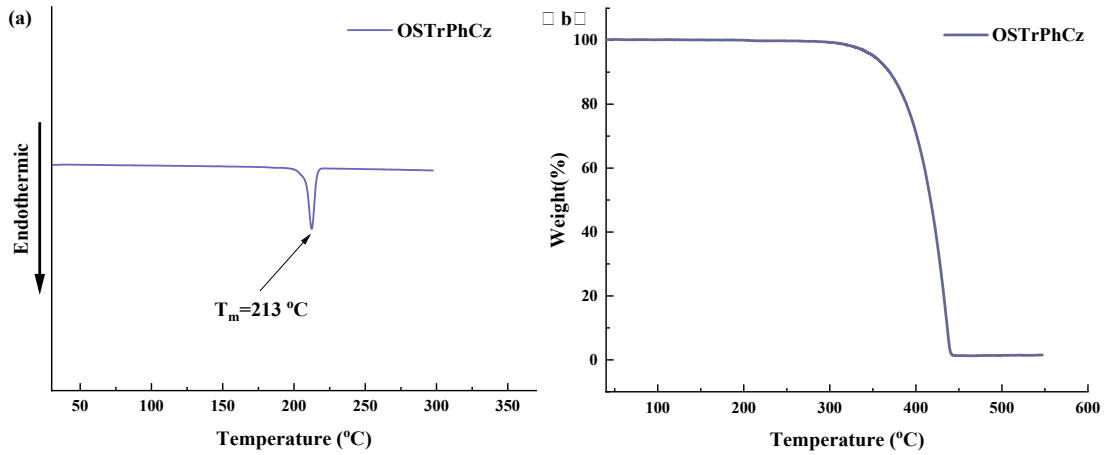

Figure S11. The DSC (a) and TGA (b) curves of emitter **OSTrPhCz** in solid powder state

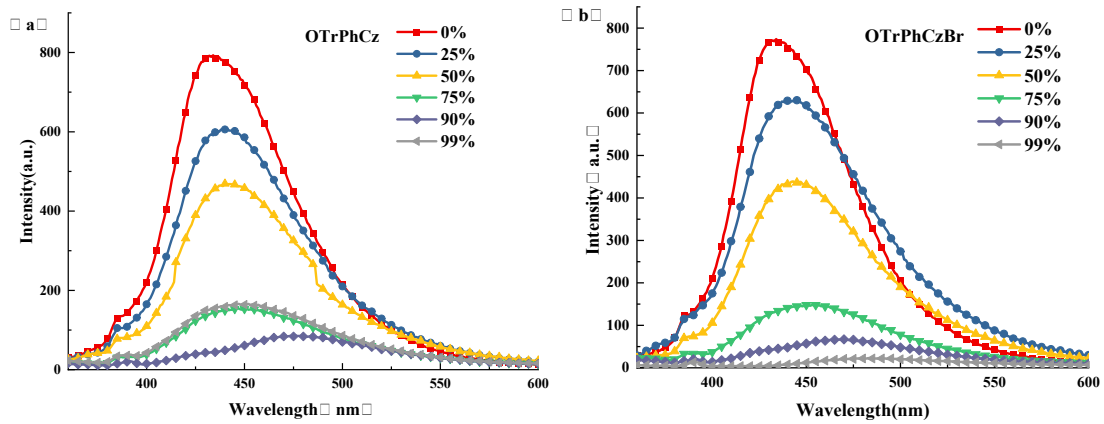

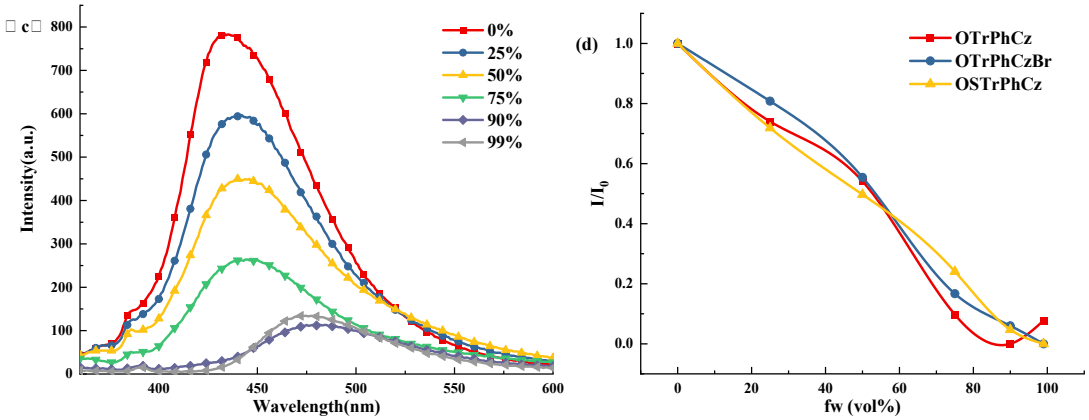

Figure S12. Photoluminescence emission spectra of emitters **OTrPhCz** (a), **OTrPhCzBr** (b) and **OSTrPhCz** (c) in a mixed solution of tetrahydrofuran and water with different water contents (F_w), (d) Emission intensity trend graph with water content (I/I_0: relative emission intensity)

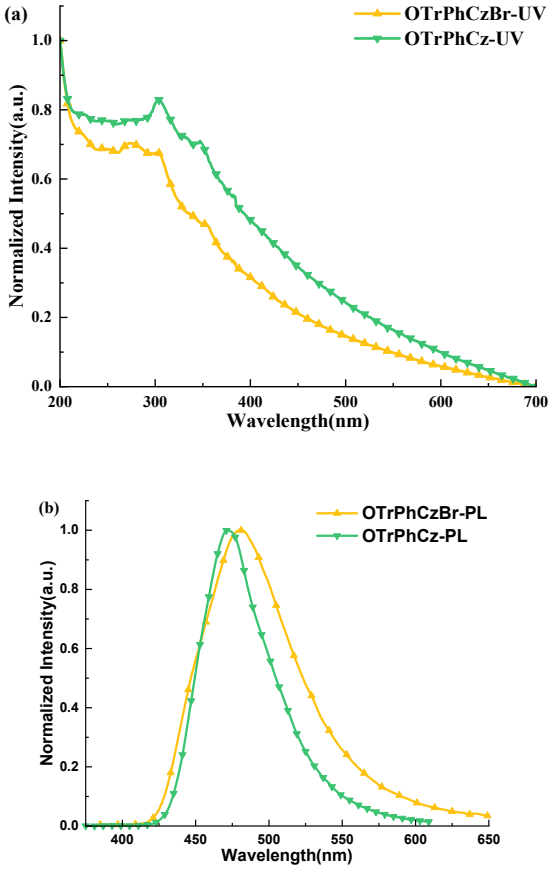

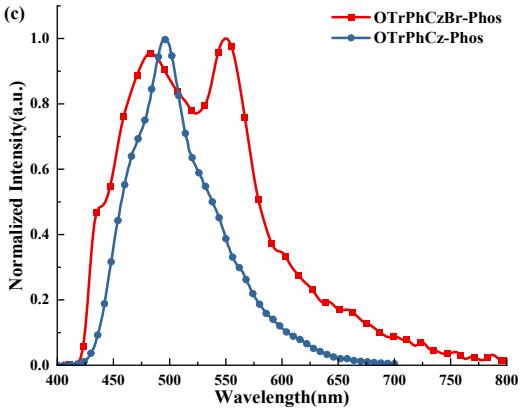

Figure S13. The normalized UV-vis absorption spectra (a), PL spectra (b) and phosphorescence spectra (c) of emitters **OTrPhCzBr** and **OTrPhCz** in the powder states

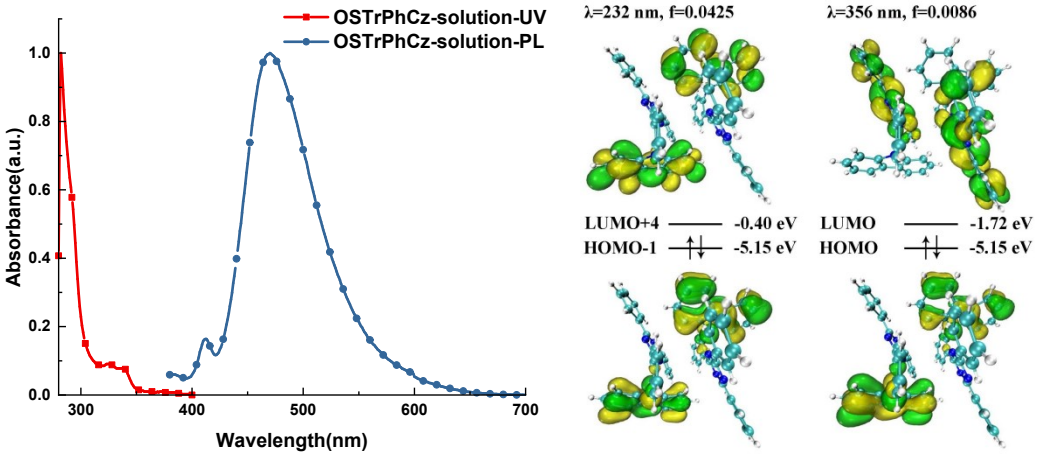

Figure S14. The normalized UV-vis absorption and PL emission spectra (left) of emitter **OSTrPhCz** in toluene (10^{-5} mol/L) solution. Calculated orbital energy levels and transition illustrations (right) of **OSrPhCz** by TDDFT at the B3LYP/6-31G(d) level (isovalue=0.02).

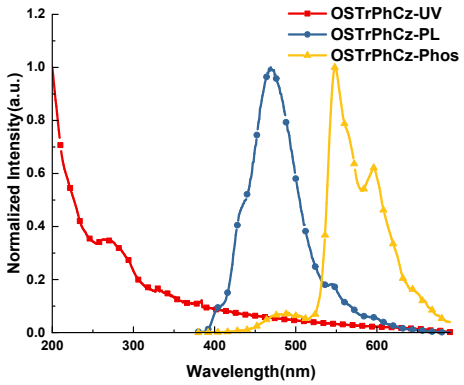

Figure S15. The normalized UV-vis absorption spectra, PL emission spectra and phosphorescence spectra of emitters **OSTrPhCz** in the powder states

In order to more clearly understand the electron excitation caused by the orbital

transition, the scheme of the specific orbital transition of the three emitters were shown here, mainly including the orbital transition illustrations corresponding to the lowest five excitations and the maximum excitation, as shown in Figures S16- S18. It can be seen that only the emitter **OSTrPhCz** occurs π-π* orbital transition at a low excitation wavelength, and the other cases are charge transfer transitions.

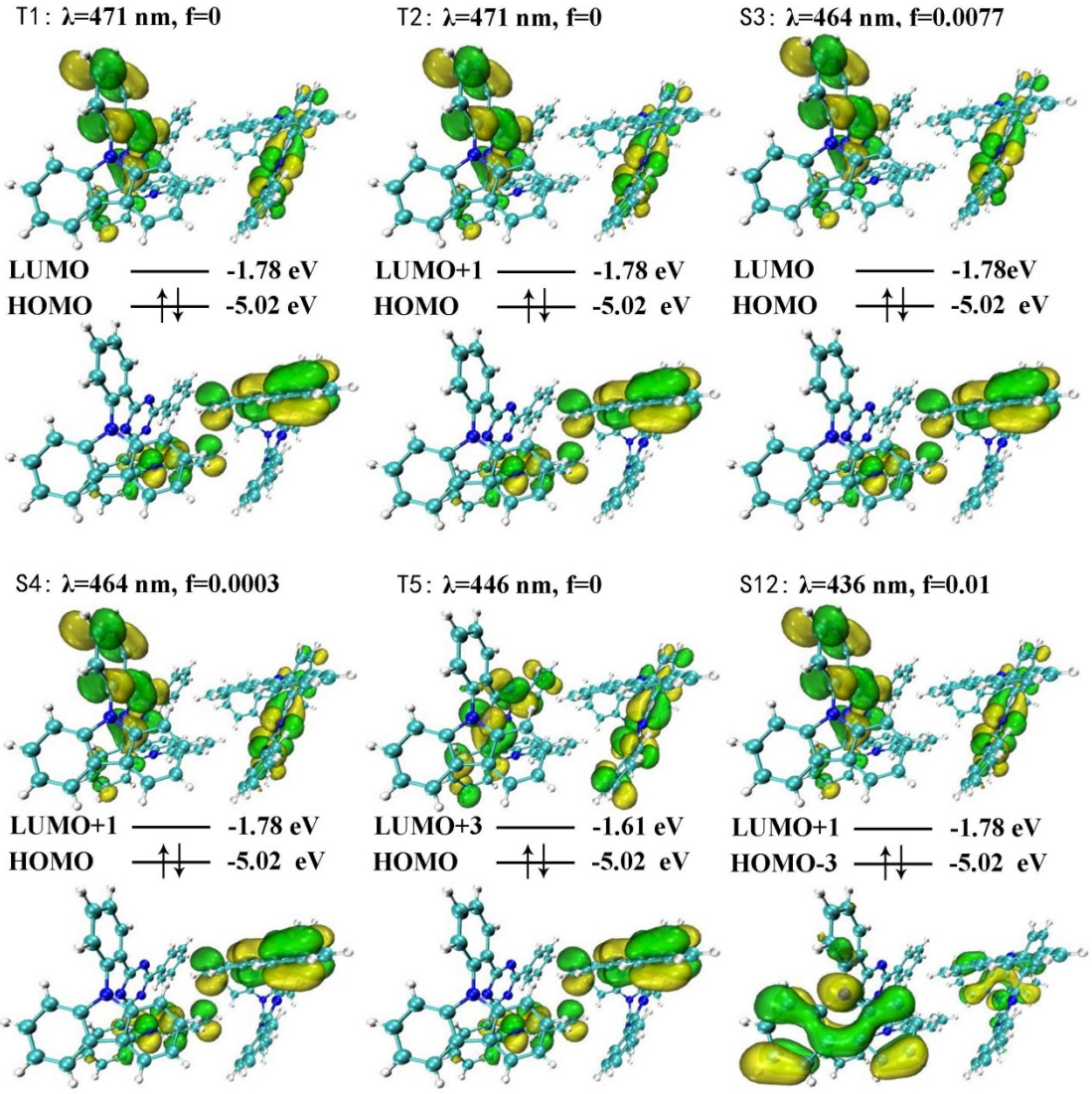

Figure S16. Calculated certain orbital energy levels and transition illustrations of **OTrPhCz** by TDDFT at the B3LYP/6-31G(d) level (isovalue=0.02).

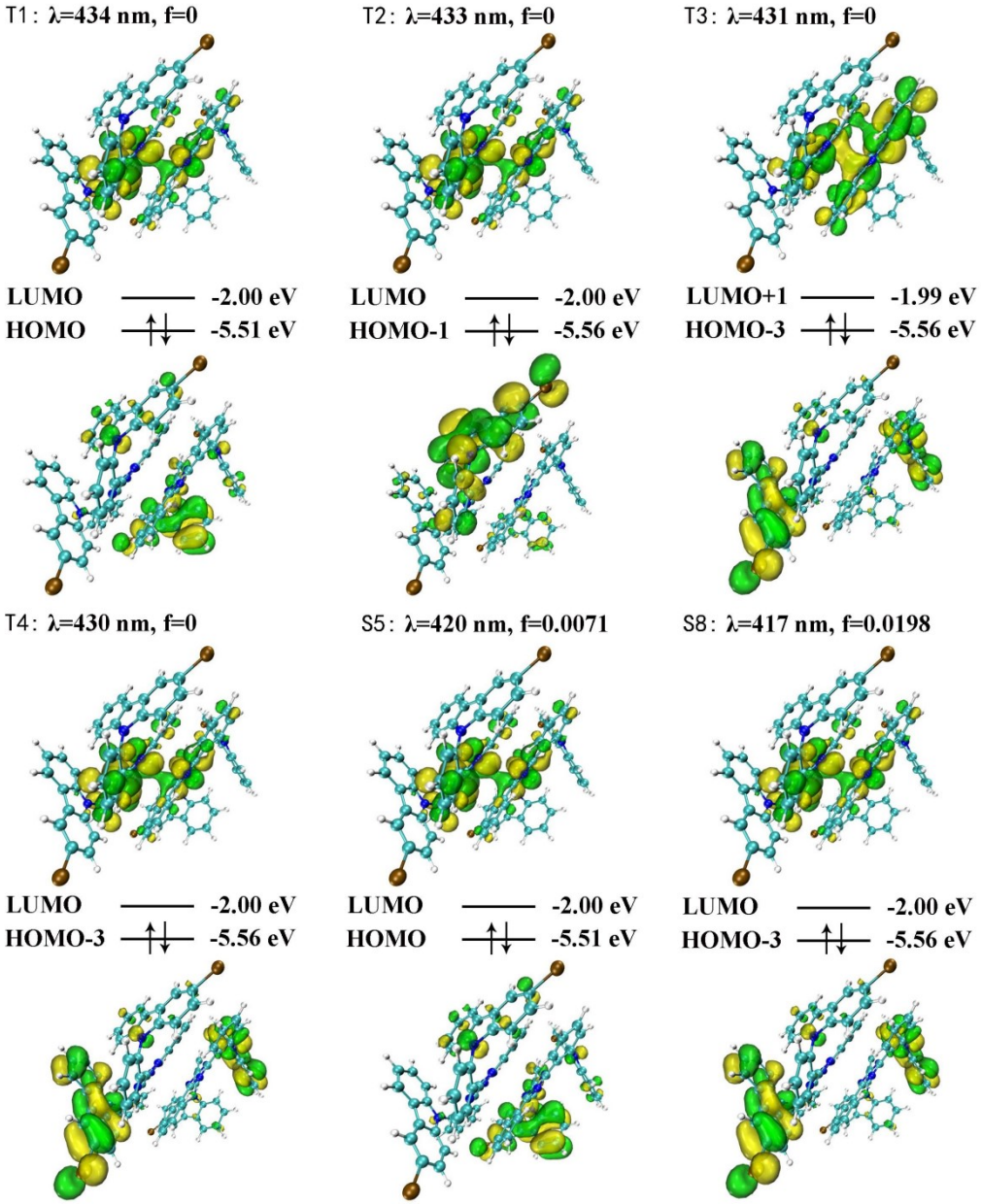

Figure S17. Calculated certain orbital energy levels and transition illustrations of **OTrPhCzBr** by TDDFT at the B3LYP/6-31G(d) level (isovalue=0.02).

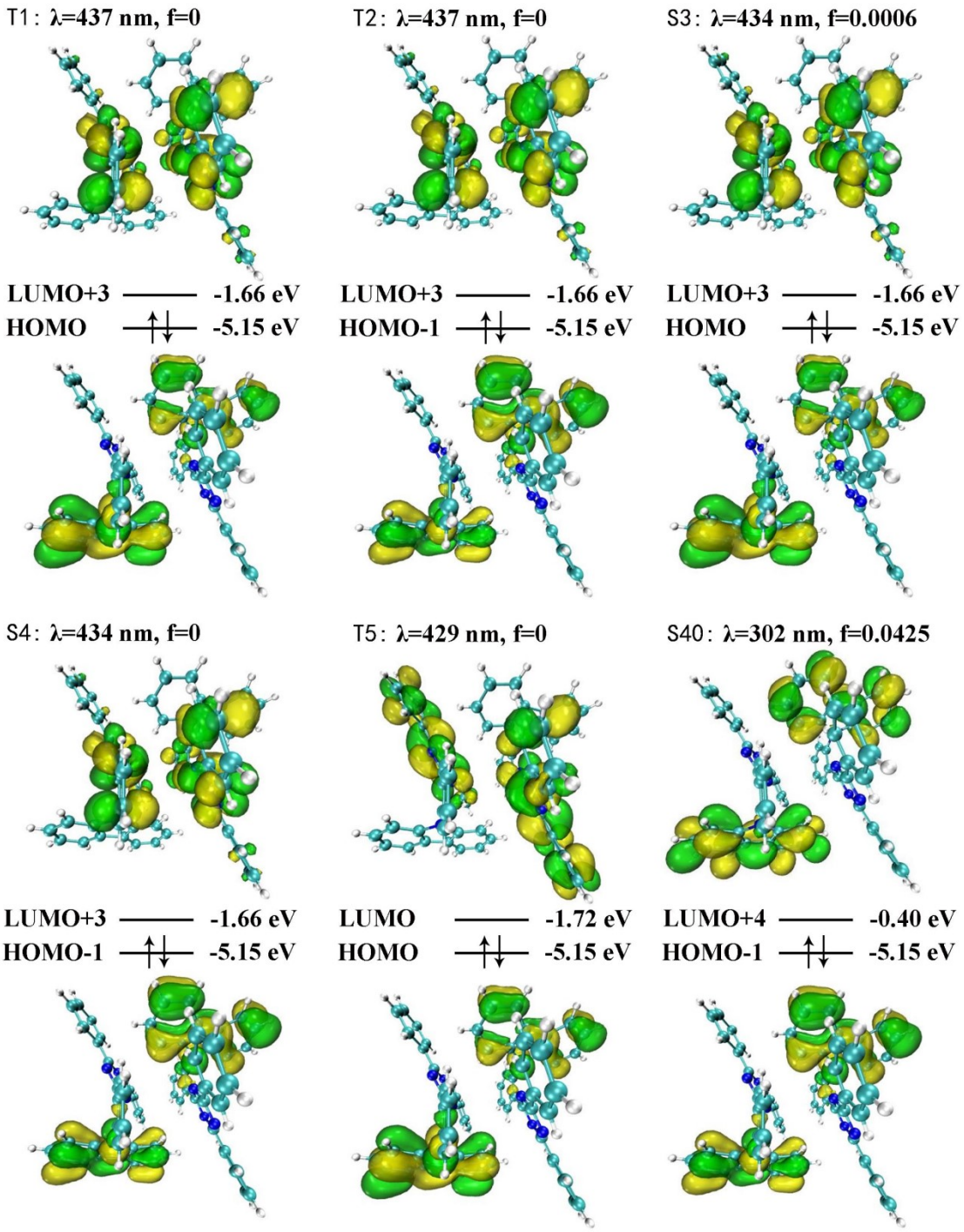

Figure S18. Calculated certain orbital energy levels and transition illustrations of **OSTrPhCz** by TDDFT at the B3LYP/6-31G(d) level (isovalue=0.02).

The DFT calculated phosphorescence emission spectra of **OTrPhCzBr, OTrPhCz,** and **OSTrPhCz** are given in Figure S19. They were calculated by TDDFT based on the optimized geometries of low-lying triplet (T_1) excited state for emitters.

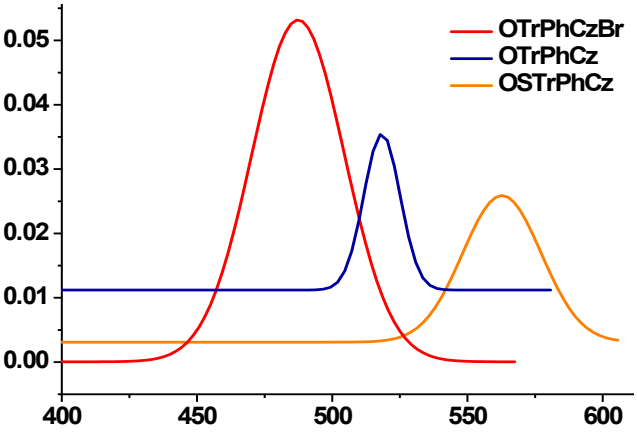

Figure S19. Calculated phosphorescence emission spectra of **OTrPhCzBr, OTrPhCz,** ans **OSTrPhCz** at the B3LYP/6-31G(d) level.

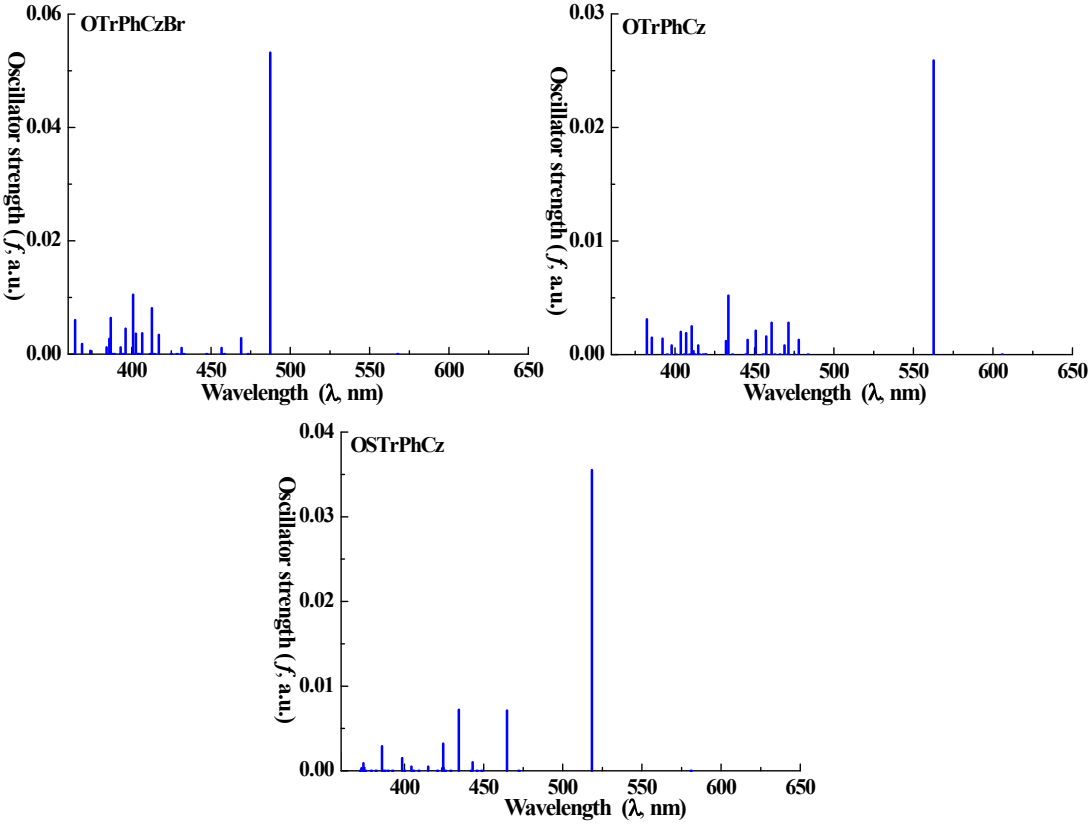

Figure S20. Calculated oscillator strength(*f*) - excitation wavelength(λ) chart based T_1 excited states of **OTrPhCzBr, OTrPhCz,** and **OSTrPhCz** at the B3LYP/6-31G(d) level.

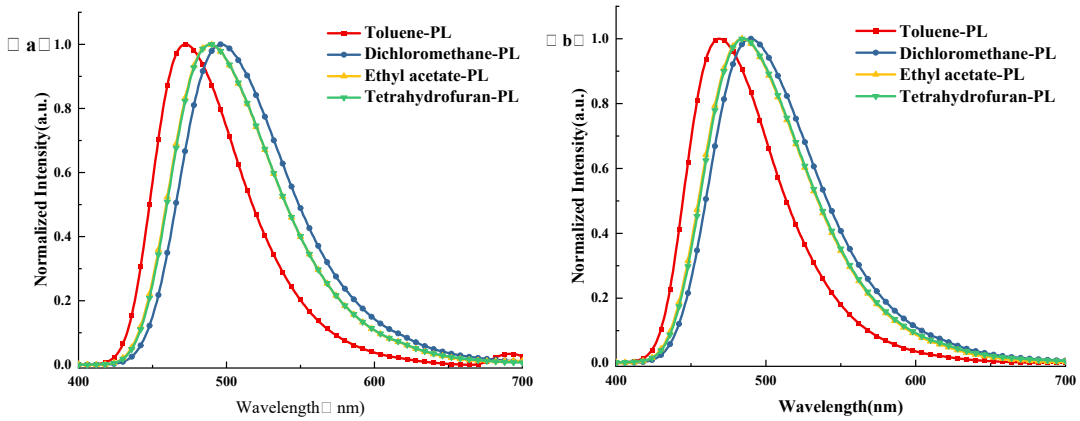

Figure S21. The normalized PL emission spectra of emitters **OTrPhCz** (a) and **OTrPhCzBr** (b) in different polar solvents at a concertation of 10^{-5} mol/L

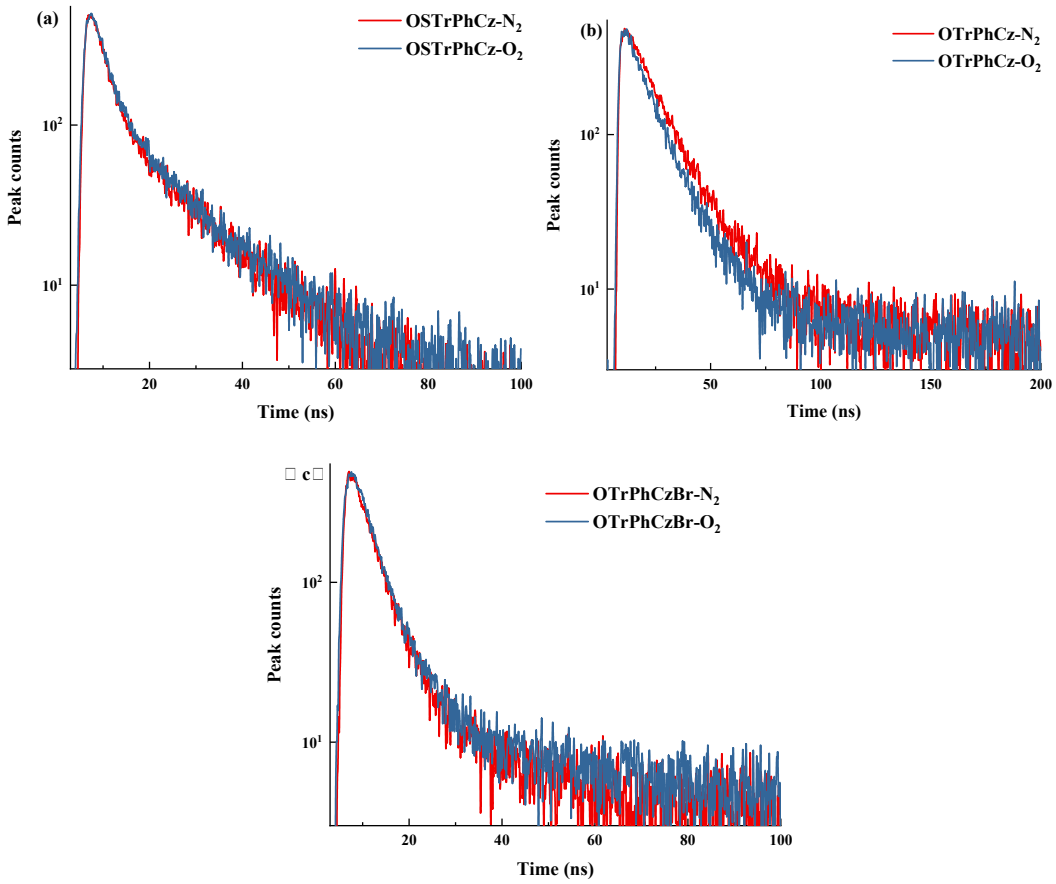

Figure S22. Transient PL decay curves of emitters **OSTrPhCz** (a), **OTrPhCz** (b) and **OTrPhCzBr** (c) solid powder under aerobic and anaerobic conditions at room temperature

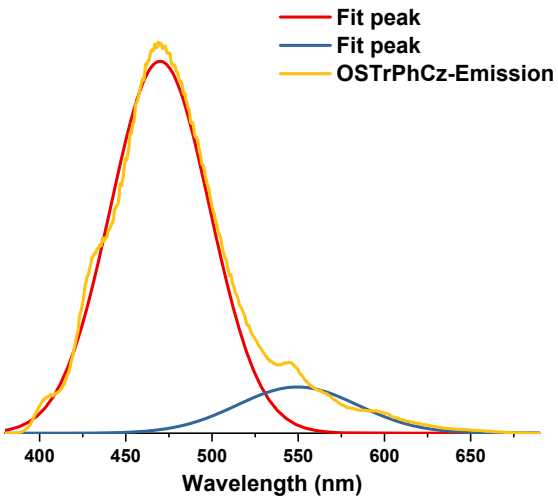

Figure S23. The peak-splitting diagram of **OSTrPhCz** PL spectra in solid powder state

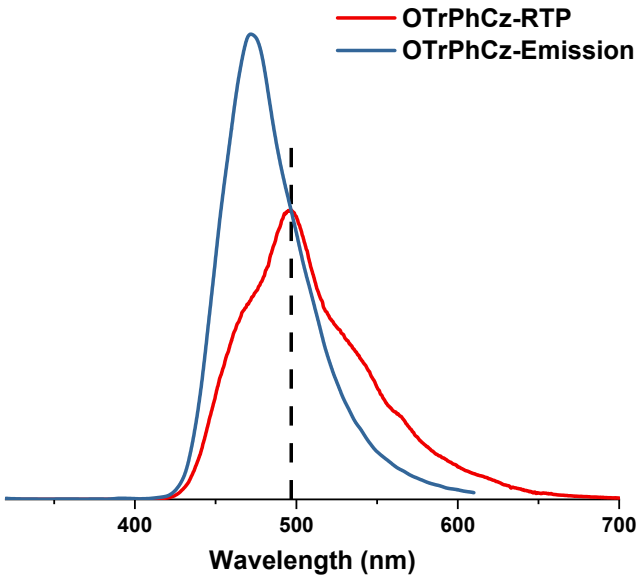

Figure S24. The peak-splitting diagram of **OTrPhCz** PL spectra in solid powder state

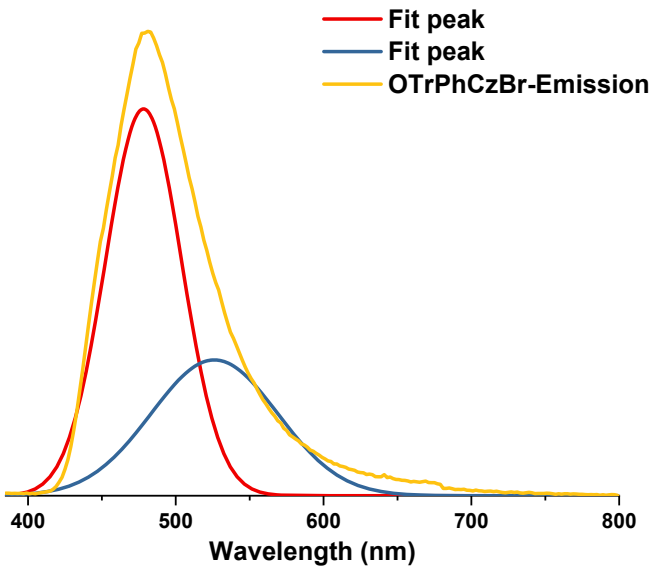

Figure S25. The peak-splitting diagram of **OTrPhCzBr** PL spectra in solid powder state

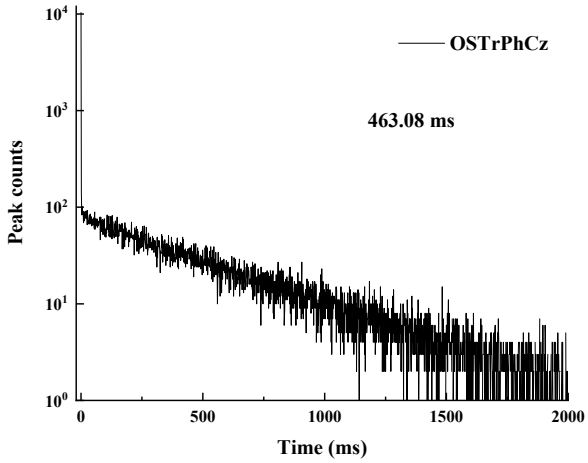

Figure S26. Photo-attenuation curves of emitters **OSTrPhCz** in the solid powder state

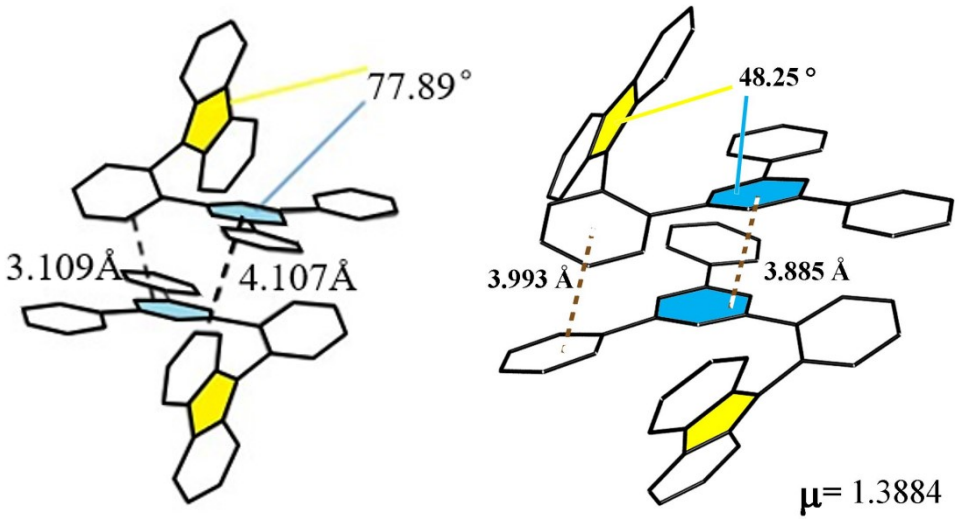

Figure S27. Crystal structure (left) and optimized geometry (right) of the emitter **OSTrPhCz**. m represents total dipole moment of the molecule, which is 1.3884, so **OSTrPhCz** has maximum phosphorescence emission intensity among three emitters

Table S1 Summary of PL lifetime data of emitters **OTrPhCz**, **OTrPhCzBr** and **OSTrPhCz** in solid powder states under aerobic and anaerobic conditions at room temperature

	τ_1/τ_2 (N_2)	τ_1/τ_2 (O_2)
OSTrPhCz	3.02/16.53 ns	3.18/15.47 ns
OTrPhCz	10.99/29.87 ns	13.92 ns
OTrPhCzBr	4.28/21.25 ns	0.36/4.65 ns

Table S2. The single crystal data of emitters **OTrPhCz**, **OTrPhCzBr** and **OSTrPhCz**

Identification code	**OTrPhCz**	**OTrPhCzBr**	**OSTrPhCz**
Empirical formula	C45H29N5	C45H27 Br2N5	C33H22N4
Formula weight	639.73	797.53	473.48
Temperature/K	296.53	105.13	294.5
Crystal system	monoclinic	monoclinic	triclinic
Space group	P21/n	P21/n	P-1
a/Å	12.694(7)	9.062(10)	9.9328(18)
b/Å	13.142(7)	16.892(2)	11.392(2)
c/Å	20.329(9)	22.899(3)	12.329(2)
α /°	90	90	96.567(5)
β /°	105.108(13)	94.139(3)	112.391(4)
γ /°	90	90	101.087(4)
Volume/Å3	3274(3)	3496.1(7)	1239.4(4)
Z	4	4	2

ρ calcg/cm3	1.298	1.515	1.272
μ /mm-1	0.077	2.361	0.076
F(000)	1336.0	1608.0	496.0
Radiation	MoKα (λ = 0.71073)	MoKα (λ = 0.71073)	MoKα (λ = 0.71073)
2Θ range for data collection/°	4.544 to 54.968	4.306 to 52.616	4.534 to 56.564
Index ranges	-16 ⩽ h ⩽ 16, -17 ⩽ k ⩽ 16, -21 ⩽ l ⩽ 26	-10 ⩽ h ⩽ 11, -21 ⩽ k ⩽ 9, -28 ⩽ l ⩽ 28	-12 ⩽ h ⩽ 13, -15 ⩽ k ⩽ 15, -16 ⩽ l ⩽ 12
Reflections collected	26932	20242	10258
Independent reflections	7509 [Rint = 0.0362, Rsigma = 0.0369]	7062 [Rint = 0.0499, Rsigma = 0.0579]	6014 [Rint = 0.0366, Rsigma = 0.0661]
Data/restraints/parameters	7509/0/451	7062/0/488	6014/0/334
Goodness-of-Fit on F2	1.035	1.100	1.021
Final R indexes [I>=2σ (I)]	R1 = 0.0517, wR2 = 0.1181	R1 = 0.1093, wR2 = 0.2517	R1 = 0.0752, wR2 = 0.1601
Final R indexes [all data]	R1 = 0.0896, wR2 = 0.1387	R1 = 0.1278, wR2 = 0.2593	R1 = 0.1139, wR2 = 0.1779
Largest diff. peak/hole / e Å-3	0.18/-0.22	0.64/-0.94	0.24/-0.24

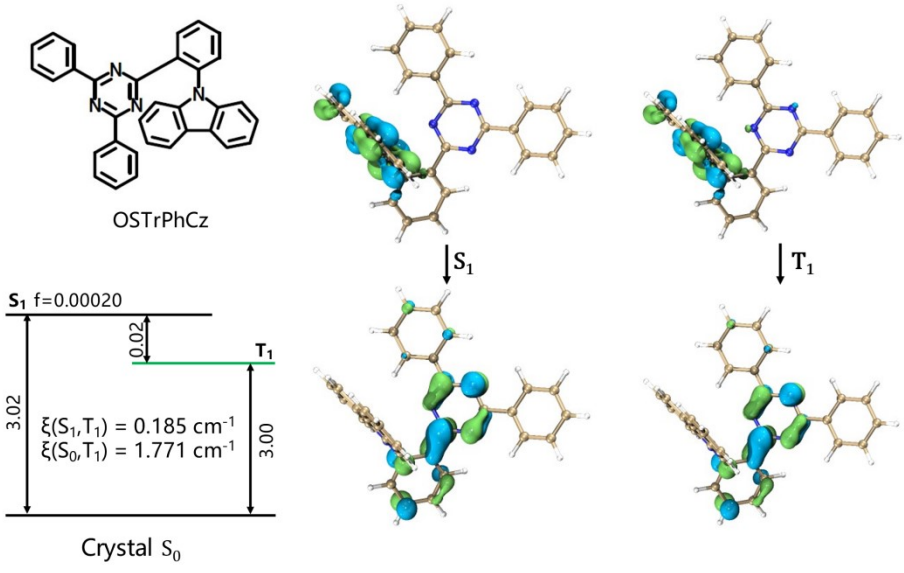

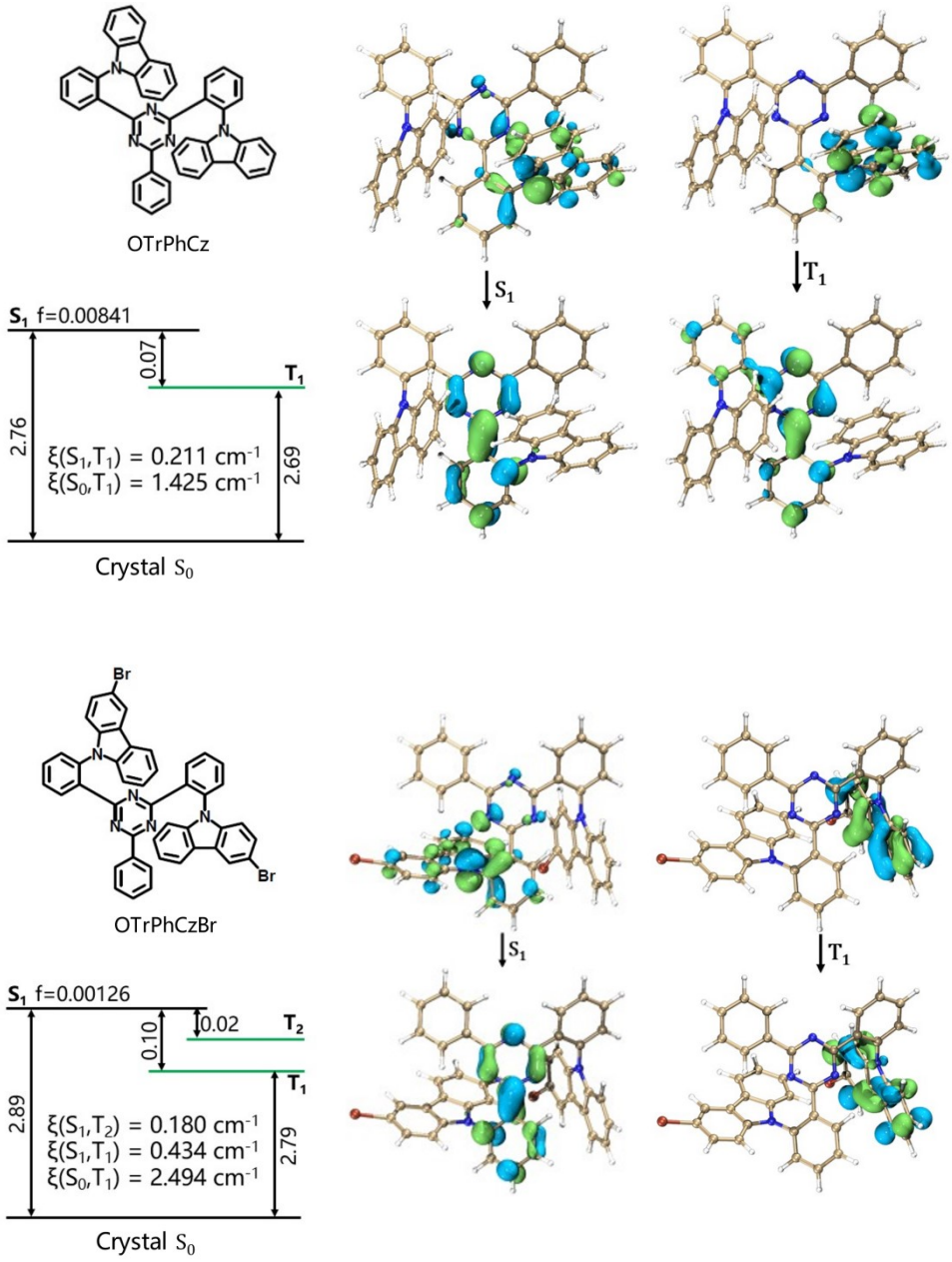

Figure S28. The calculated spin-orbit coupling constant, calculated energy diagram, and spin-orbital coupling (ξ) in the crystalline phase of **OTrPhCz**, **OTrPhCzBr** and **OSTrPhCz**.

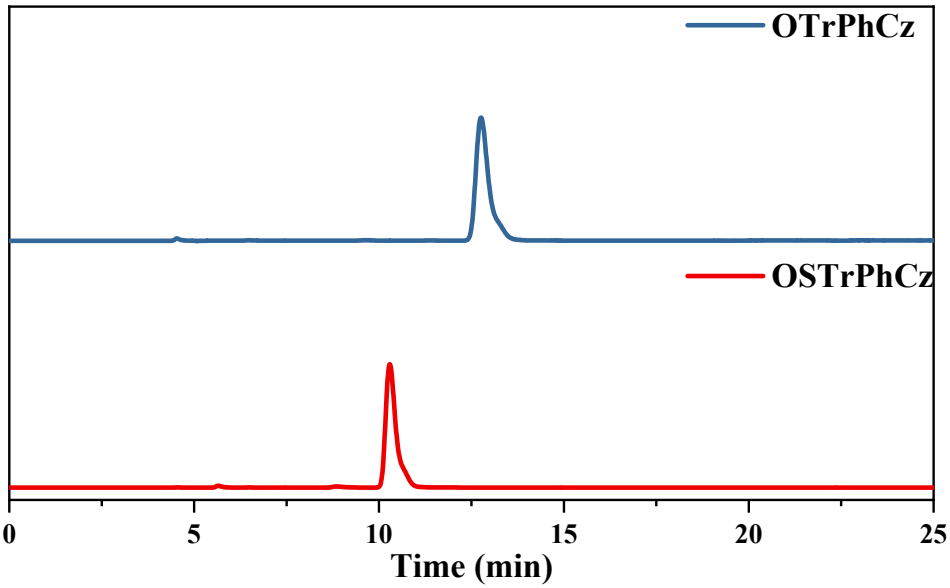

Figure S29. The HPLC spectra collected with acetonitrile as mobile phase at 0.8 mL/min and at 35 °C, which were monitored at 288 nm for **OTrPhCz** and 282 nm for **OSTrPhCz**.

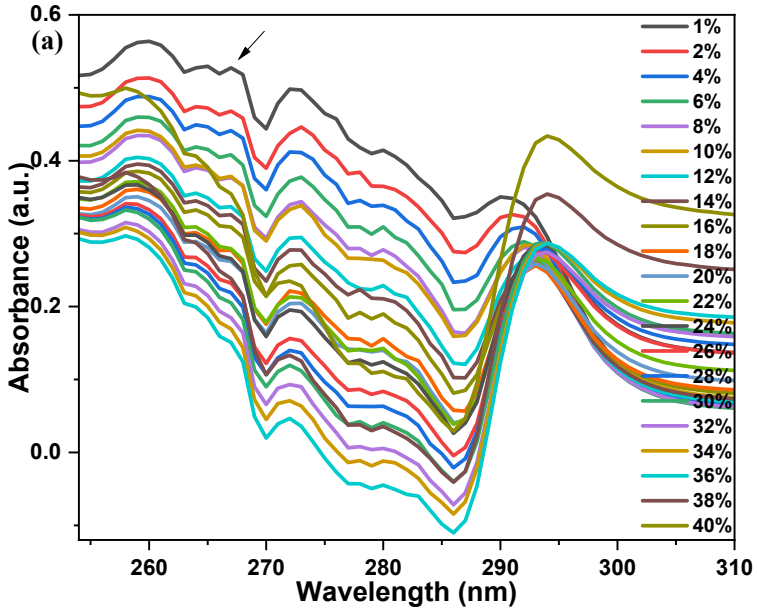

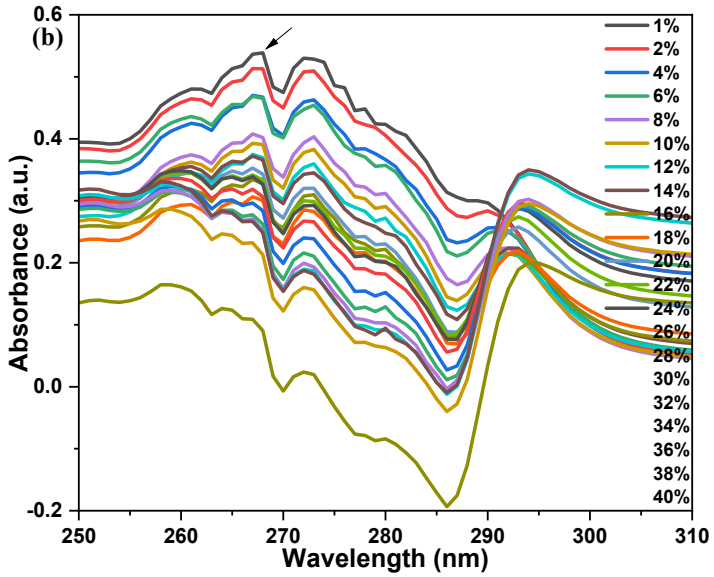

Figure S30. The UV-vis absorption spectra of **OTrPhCz**(a) and **OSTrPhCz**(b) (10 μM) measured in the mixture solvents of tetrahydrofuran and water with different water volumes

Table S3. Aggregation structures of **OTrPhCz**, **OTrPhCzBr** and **OSTrPhCz** cystals investigated by Frenkel exciton theory through the nearest neighboring dimers. When the splitting energy (Δε) > 0, this pair of dimer belongs to H-aggregation (in red), and when Δε < 0, it is J-aggregation (in black).

Compounds	Dimer	*α* (°)	θ_1(°)	θ_2(°)	M (Debye)	r (Å)	Δε (eV)
	4 0	0.006393171	63.65510274	63.65282152	0.143684098	22.78400787	8.92738E-07
	4 1	0.009489505	77.85244466	77.84457896	0.143684098	27.11763783	1.12211E-06
	4 2	0.006403858	63.65511491	63.6539265	0.143684098	11.39201041	7.1423E-06
	4 3	0.009218502	87.89461605	87.88655113	0.143684098	17.71743338	4.62129E-06
	4 5	0.009218502	110.9316359	110.9224406	0.143684098	12.32899146	8.50015E-06
	4 6	0.006403858	88.34311989	88.3449825	0.143684098	16.4911368	5.73975E-06
	4 7	0.009218502	101.894607	101.8895702	0.143684098	19.05637806	3.25411E-06
OSTrPhCz	4 8	0	117.4492186	117.4492186	0.143684098	9.932800055	9.54722E-06
	4 9	0.009218502	135.6673024	135.6608056	0.143684098	12.55878583	-6.96716E-06
	4 10	72.45478526	76.99801008	89.49005126	0.143684098	22.40229619	6.78176E-07
	4 11	72.44925987	90.0744443	99.37572677	0.143684098	11.76640124	4.76703E-06
	4 12	72.44916261	149.5638564	133.3118266	0.143684098	5.881216889	-0.000186838
	4 13	72.44925987	105.4704405	75.79106148	0.143684098	17.22243902	2.51568E-06

	4 14	72.44916261	142.1752225	80.05443792	0.143684098	12.21613009	1.00622E-05
	□	□	□	□	□	□	□

Compounds	Dimer	α (°)	θ_1(°)	θ_2(°)	M (Debye)	r (Å)	Δε (eV)
OTrPhCz	13 0	44.61314215	90.36847137	67.79604934	0.360107151	10.50159667	0.000100655
	13 1	44.61314215	107.079463	122.2179215	0.360107151	13.32453189	1.65902E-05
	13 2	78.63158819	47.77767219	122.4653243	0.360107151	12.99544873	9.44884E-05
	13 3	78.63158819	106.1138356	168.12932	0.360107151	13.54855675	-4.02615E-05
	13 4	78.63158819	48.82486868	56.50503946	0.360107151	7.42328201	-0.000353816
	13 5	78.63158819	155.5749415	105.1720617	0.360107151	8.353850499	-0.000143965
	13 6	36.15113149	54.34785537	90.40410047	0.360107151	21.69712247	1.30101E-05
	13 7	36.15113149	89.59589713	125.6521422	0.360107151	21.69712219	1.30101E-05
	13 8	36.15113149	39.09702072	70.99497931	0.360107151	11.33981615	5.47712E-06
	13 9	36.15113149	109.0050168	140.9029754	0.360107151	11.33981559	5.47714E-06
	13 10	36.15113149	61.62447344	43.68958151	0.360107151	10.42559337	-3.19684E-05
	13 11	36.15113149	136.3104147	118.3755227	0.360107151	10.42559276	-3.19684E-05
	13 12	0	72.36417305	72.36417305	0.360107151	12.69399977	5.74254E-05
	13 14	8.53774E-07	107.635827	107.635827	0.360107151	12.6940012	5.74254E-05
	□	□	□	□	□	□	□

Compounds	Dimer	α (°)	θ_1(°)	θ_2(°)	M (Debye)	r (Å)	Δε (eV)
OTrPhCzBr	7 0	72.45936892	75.55815692	33.70780037	0.425023293	12.60174883	-3.62231E-05
	7 1	72.45936892	146.2914965	104.4425962	0.425023293	12.60174819	-3.62261E-05
	7 2	72.45936892	46.64887836	64.9373454	0.425023293	12.27497538	-6.97134E-05
	7 3	72.45936892	115.0611991	133.3508926	0.425023293	12.27497472	-6.97072E-05
	7 4	8.53774E-07	64.20231411	64.20231411	0.425023293	19.16923383	1.38429E-05
	7 5	8.53774E-07	125.6648153	125.6648153	0.425023293	9.062000155	-6.01273E-06
	7 6	0	36.23039207	36.23039207	0.425023293	16.89200044	-4.46019E-05
	7 8	115.1193373	63.20466773	146.8770352	0.425023293	18.91941832	2.36123E-05
	7 9	115.1223327	59.58113419	136.624884	0.425023293	19.31117909	2.13072E-05
	7 10	115.1193373	114.6553071	94.82616782	0.425023293	12.21817807	-6.5589E-05
	7 11	115.1223327	107.4733253	86.50772301	0.425023293	12.81643958	-3.96523E-05
	7 12	115.1193373	44.3355869	126.9771547	0.425023293	19.31118519	2.71594E-05
	7 13	115.1223327	37.24384157	121.2249348	0.425023293	18.91941493	2.71251E-05
	7 14	115.1193373	89.16570543	75.5347974	0.425023293	12.81644877	-4.67029E-05
	7 15	115.1223327	83.25400606	65.79406065	0.425023293	12.21817282	-7.04481E-05
	7 16	172.1425228	50.60938683	136.3340339	0.425023293	7.214087569	0.000232498
	7 17	172.1425228	142.8894477	32.21500785	0.425023293	11.34558101	0.000159799

	7 18	172.1425228	20.64467895	153.6999372	0.425023293	10.53833929	0.000294456
	7 19	172.1425228	105.9459349	66.92577155	0.425023293	13.70166938	-5.86047E-05

[S1] M. J. Frisch, G. W. Trucks, H. B. Schlegel, G. E. Scuseria, M. A. Robb, J. R. Cheeseman, G. Scalmani, V. Barone, G. A. Petersson, H. Nakatsuji, X. Li, M. Caricato, A. V. Marenich, J. Bloino, B. G. Janesko, R. Gomperts, B. Mennucci, H. P. Hratchian, J. V. Ortiz, A. F. Izmaylov, J. L. Sonnenberg, D. Williams-Young, F. Ding, F. Lipparini, F. Egidi, J. Goings, B. Peng, A. Petrone, T. Henderson, D. Ranasinghe, V. G. Zakrzewski, J. Gao, N. Rega, G. Zheng, W. Liang, M. Hada, M. Ehara, K. Toyota, R. Fukuda, J. Hasegawa, M. Ishida, T. Nakajima, Y. Honda, O. Kitao, H. Nakai, T. Vreven, K. Throssell, J. A. Montgomery, Jr., J. E. Peralta, F. Ogliaro, M. J. Bearpark, J. J. Heyd, E. N. Brothers, K. N. Kudin, V. N. Staroverov, T. A. Keith, R. Kobayashi, J. Normand, K. Raghavachari, A. P. Rendell, J. C. Burant, S. S. Iyengar, J. Tomasi, M. Cossi, J. M. Millam, M. Klene, C. Adamo, R. Cammi, J. W. Ochterski, R. L. Martin, K. Morokuma, O. Farkas, J. B. Foresman, and D. J. Fox, Gaussian, Inc., Wallingford CT, 2016.

[S2] Humphrey W., Dalke A. and Schulten K., VMD: Visual molecular dynamics, J. Molec. Graphics, 1996, 14, 1, 33-38.

[S3] Lu Tian, Chen Feiwu, Multiwfn: A multifunctional wavefunction analyzer, J. Comput. Chem., 2012, 33, 5, 580-592.